Micelles

DOI: 10.1002/ange.201206197

Nanosized Poly(ethylene glycol) Domains within Reverse Micelles Formed in CO_2**

Zhimin Xue, Jianling Zhang, Li Peng, Jianshen Li, Tiancheng Mu, Buxing Han,* and Guanying Yang*

The liquid at nanometer scale differs substantially from bulk liquid, which is of particular significance for different applications.[1] As one of the most efficient ways, reverse micelles have been widely utilized in forming liquid domains at the nanometer scale.[2] For example, nanosized water domains are formed in reverse micelles, which can be used as nanoreactors for chemical reactions,[3] material synthesis,[4] extraction,[5] and biochemistry research.[6] Recently, room-temperature ionic liquids (ILs) have been reported to form nanosized domains in reverse micelles,[7] which have found applications in material synthesis[7c,8] and chemical reactions.[9]

Poly(ethylene glycol) (PEG) with a small molecular weight ($< 800\ g\,mol^{-1}$) is in the liquid state at room temperature. Liquid PEG is usually regarded as green solvent, because it is economical, environmentally benign, biocompatible, and its properties are tunable by changing the molecular weight.[10] Owing to these special properties, liquid PEGs have been widely used in various fields, such as materials science,[11] chemical reactions,[12] electrochemistry,[13] pharmaceutical industry,[14] and others.

Herein we report for the first time the formation of nanosized PEG domains in reverse micelles by using supercritical CO_2 as the continuous phase. Supercritical CO_2 is readily available, inexpensive, nontoxic, nonflammable, and the physical properties can be adjusted continuously by pressure and temperature.[15] Therefore, the system combines the advantages of both PEG and supercritical CO_2. With the aid of surfactant *N*-EtFOSA ($C_2H_5NHSO_2C_8F_{17}$, see Figure S1 in the Supporting Information for its molecular structure), the nanosized PEG domains are formed in CO_2. The PEG domains are "tunable", because their size and property can be easily changed by controlling the PEG content. Furthermore, to demonstrate their potential applications, the nanosized PEG domains have been utilized as nanoreactors to synthesize highly dispersed gold nanocrystals.

The phase behavior of the PEG-400/*N*-EtFOSA/CO_2 systems was observed at different pressures and temperatures. The surfactant concentration was fixed at $0.05\ g\,mL^{-1}$. The cloud-point pressure is the minimum pressure at which the PEG-400/*N*-EtFOSA/CO_2 system keeps in one phase region. In other words, when the pressure is lower than the cloud-point pressure, phase separation occurs. The dependence of the cloud-point pressure of the PEG-400/*N*-EtFOSA/CO_2 system on the molar ratio of PEG-400 to surfactant (W_0^{total}) at different temperatures is shown in Figure S2 in the Supporting Information. It is known that a small amount of PEG can be solubilized in CO_2 at high pressure.[16] In this work the amount of PEG-400 solubilized in pure CO_2 at different pressures and temperatures was determined (Table S1 in the Supporting Information), and a comparison for the PEG solubility in pure CO_2 and in the *N*-EtFOSA/CO_2 system is shown in Figure S3 in the Supporting Information. It is clear that the PEG solubility is enhanced significantly with the addition of surfactant *N*-EtFOSA. This enhanced solubility indicates that a sufficient amount of PEG is solubilized in reverse micelles, that is, PEG-in-CO_2 microemulsions are formed. The molar ratio of PEG solubilized in reverse micelles to surfactant is denoted as W_0^{corr}, which is obtained by subtracting the amount of PEG in bulk CO_2 from the total amount of loading PEG. Figure 1 shows the dependence of cloud-point pressure of the PEG-400/*N*-EtFOSA/CO_2 system on W_0^{corr} at different temperatures. Evidently, the cloud-point pressure increases with increasing ratio W_0^{corr}. The cloud-point pressure increases, because with a higher concentration

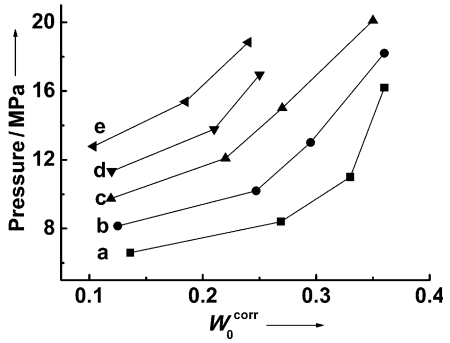

Figure 1. Dependence of the cloud-point pressure of the PEG-400/*N*-EtFOSA/CO_2 systems on the ratio W_0^{corr} at 298.2 K (a), 303.2 K (b), 308.2 K (c), 313.2 K (d), and 318.2 K (e). The surfactant concentration is $0.05\ g\,mL^{-1}$.

[*] Z. Xue, Prof. J. Zhang, L. Peng, J. Li, Dr. T. Mu, Prof. B. Han, G. Yang
Beijing National Laboratory for Molecular Sciences, CAS Key Laboratory of Colloid and Interface and Chemical Thermodynamics
Institute of Chemistry, Chinese Academy of Sciences
Department of Chemistry, Renmin University of China (China)
E-mail: zhangjl@iccas.ac.cn
hanbx@iccas.ac.cn

[**] We thank the National Natural Science Foundation of China (21173238, 21133009, 21073207, 21021003, U1232203), Ministry of Science and Technology of China (2009CB930802), Chinese Academy of Sciences (KJCX2.YW.H16). We are also grateful to Prof. Zhonghua Wu and Zhihong Li of Beijing Synchrotron Radiation Facility (BSRF) for their help on small-angle X-ray scattering experiments.

Supporting information for this article is available on the WWW under http://dx.doi.org/10.1002/anie.201206197.

of PEG-400, a higher density of CO_2 is needed to form the microemulsions for solubilizing PEG-400, similar to the water-in-CO_2 microemulsions.[17] Moreover, as shown in Figure 1, the cloud-point pressure increases with increasing temperature at the same ratio W_0^{corr}; this increase can be attributed to the decreased density of CO_2 at higher temperatures.[7c] At the experimental conditions, the maximum ratio W_0^{corr} can reach 0.36. At this W_0^{corr} value, the PEG-to-surfactant weight ratio is equivalent to the water-to-surfactant weight ratio of water-in-CO_2 reverse micelles with a water-to-surfactant molar ratio of about 8, since the molecular weights of PEG-400 and water are 400 and 18 g mol^{-1}, respectively. The above results confirm that PEG can be well solubilized in the *N*-EtFOSA reverse micelles when the pressure is higher than the cloud-point pressure.

The microstructure of the PEG-400/*N*-EtFOSA/CO_2 microemulsion was investigated by small-angle X-ray scattering (SAXS).[18] Figure 2A shows the SAXS curves of the ternary systems with different W_0^{corr} values at 298.2 K and 10.50 MPa. The intensity shifts to low scattering wavevector

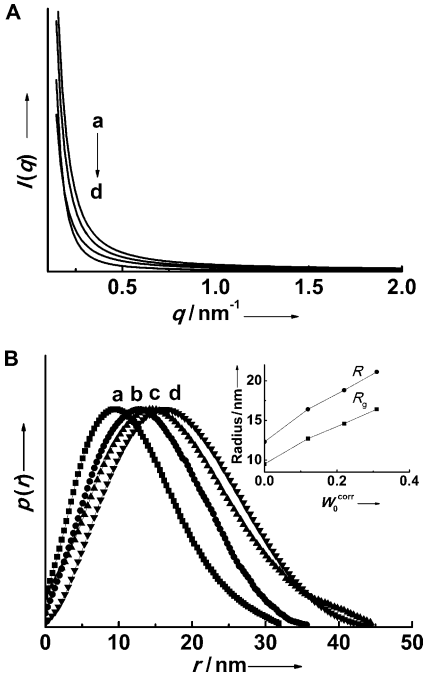

Figure 2. SAXS curves (A) and normalized pair–distance distribution function curves (B) of PEG-400/*N*-EtFOSA/CO_2 systems with W_0^{corr} values of 0 (a), 0.12 (b), 0.22 (c), and 0.31 (d) at 10.50 MPa and 298.2 K. The inset in (B) shows the dependence of gyration radius (R_g) and true radius (R) of reverse micelles on W_0^{corr} value.

(q) with increasing W_0^{corr} values, thus indicating that the reverse micelles are enlarged at higher W_0^{corr}.[19] The generalized indirect Fourier transformation (GIFT) gives the pair–distance distribution function, $p(r)$, which has been utilized to characterize the microstructure of water-in-oil reverse micelles.[19b–d] As shown in Figure 2B, the $p(r)$ curves are nearly symmetric, thus suggesting that the reverse micelles are spherical-shaped. The gyration radius R_g and the true radius R of the reverse micelles with different W_0^{corr} values were calculated from $p(r)$ functions[20] and are shown in the inset of Figure 2B. Clearly, the micellar size is increased with increasing W_0^{corr} value, thus indicating that the micelles are expanded by the addition of PEG. This result further proves the formation of the PEG-in-CO_2 microemulsions. Moreover, the SAXS curves of PEG-400/*N*-EtFOSA/CO_2 microemulsions at different pressures were determined at a W_0^{corr} value of 0.12. No obvious changes were observed with increasing pressure (Figure S4 in the Supporting Information), thus indicating the effect of pressure on the micellar size is negligible. Similarly, the water-droplet radius for the water-in-CO_2 microemulsions changes little with pressure for the microemulsions with the same W_0 value.[21]

The micropolarity of the nanosized PEG domains was investigated with a UV/Vis method using methyl orange (MO) as the probe, of which the absorption wavelength is sensitive to the microenvironment.[18b,22] As the local environment of MO becomes more polar, the maximum absorption wavelength shifts to longer wavelengths. Curves (a–c) in Figure 3 show the UV/Vis spectra of MO in PEG-400/*N*-EtFOSA/CO_2 microemulsions with different W_0^{corr} values,

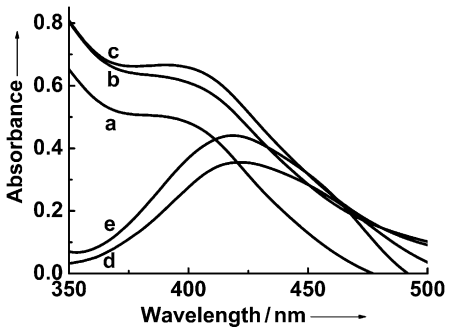

Figure 3. UV/Vis spectra of MO in PEG-400/*N*-EtFOSA/CO_2 microemulsions with W_0^{corr} values of 0.08 (a), 0.25 (b), and 0.32 (c) at 10.50 MPa and 298.2 K; (d) is the spectrum of MO in pure PEG-400; (e) is the spectrum of MO in the CO_2/PEG-400 system at 10.50 MPa.

with the pressure fixed to 10.50 MPa. The λ_{max} becomes red-shifted with increasing W_0^{corr} value. This shift is indicative of the increased micropolarity of the nanosized PEG domains with increasing W_0^{corr} value. For comparison, the UV/Vis spectra of MO in the PEG/CO_2 system without the surfactant at different pressures were also determined. The UV/Vis spectrum of MO in pure PEG-400 shows maximum absorption at 422 nm (Figure 3, curve d), which shifts to 418.5 nm at 10.50 MPa (Figure 3, curve e). The absorption maximum shifts, because CO_2 can be well dissolved in PEG[23] owing to the Lewis acid–base interaction revealed by IR absorption spectroscopy.[23c,d] The dissolution of CO_2 reduces the polarity of PEG and results in the blue shift of the absorption band. After combination of the above results, it is evident that the λ_{max} value in the microemulsions (Figure 3, curves a–c) is smaller than that of bulk PEG at the same pressure (curve e), thus indicating that the micropolarity of nanosized PEG domains is lower than that of the CO_2-saturated bulk PEG. This behavior is similar to that of the water-in-CO_2 microemulsions, in which the micropolarity of confined water

domains is lower than that of CO_2-saturated bulk water.[24] Furthermore, the UV/Vis spectra of MO in PEG-400/*N*-EtFOSA/CO_2 microemulsions with the same W_0^{corr} value at different pressures were determined (Figure S5 in the Supporting Information). The effect of pressure on the micropolarity of the nanosized PEG domains is very limited.

The nanosized PEG-400 domains in the microemulsions can be used as nanoreactors. Since PEG has been frequently used as a stabilizer for metal nanoparticles,[25] herein the synthesis of gold nanoparticles in the microemulsion was studied. $HAuCl_4$ was used as the gold precursor, which is well solubilized in PEG-400. No additional reducing agent was added to the PEG-400/*N*-EtFOSA/CO_2 system. Highly dispersed gold nanoparticles were produced with a size smaller than 10 nm (Figure 4a). Figure 4b shows that the gold nanoparticles are polyhedron crystals. The XRD pattern of the gold nanoparticles reveals the face-centered cubic structure of metallic gold (Figure S6 in the Supporting Information). These gold polyhedron nanocrystals exhibit a single absorption at 524 nm (Figure S7 in the Supporting Information), in agreement with that of gold nanoparticles of similar size.[26] To explore the formation mechanism of the gold crystals, we also investigated the gold synthesis in pure PEG and in the "dry micelles" without PEG. In pure PEG-400, the reduction of $HAuCl_4$ cannot proceed. This finding indicates that it is the surfactant that reduces the $HAuCl_4$. As is well-recognized, $HAuCl_4$ can be easily reduced by many compounds containing, for example, amine or oxyethylene groups.[27] Herein the amine head groups of the surfactant are believed to be active for reducing Au^{3+} ions to metallic Au. Moreover, in the "dry micelles" without PEG, $HAuCl_4$ cannot be solubilized in the surfactant/CO_2 system, and no product was obtained. This result suggests that the solubilization of $HAuCl_4$ in the PEG domains is crucial to the gold formation. On the basis of the above results, a mechanism for the gold formation is proposed and illustrated in Figure 4c. $HAuCl_4$ is solubilized in the nanosized PEG domains and reduced by the surfactant head groups. Owing to both the stabilization of gold particles by PEG and the confinement effect of nanosized reverse micelles, highly dispersed gold nanoparticles were formed.

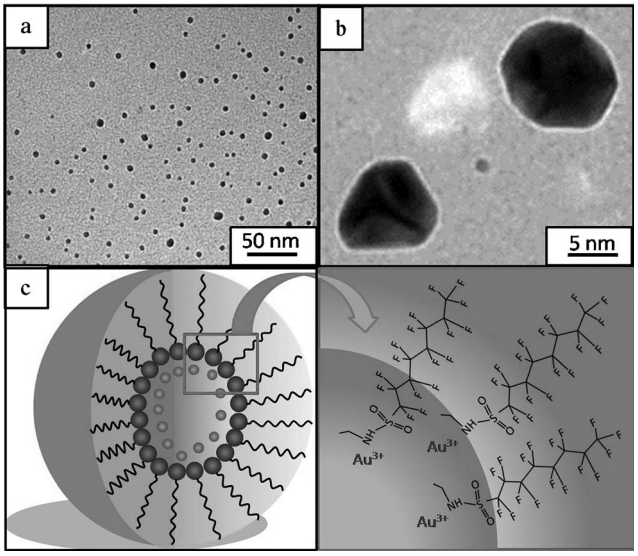

Figure 4. a, b) TEM images of gold nanoparticles obtained from PEG-400/*N*-EtFOSA/CO_2 microemulsion. c) Schematic illustration for the gold formation (~~~: surfactant; ●: Au^{3+}).

It is known that the PEGs with a molecular weight above 800 g mol^{-1} are in solid state at room temperature. Since CO_2 dissolves well in PEG and liquefies many solid PEGs,[28] herein we also determined the solubilization of PEG-1000 in the *N*-EtFOSA/CO_2 system. We found that a certain amount of PEG-1000 can be solubilized in the *N*-EtFOSA/CO_2 system. The dependence of the cloud-point pressure on the ratio W_0 at 298.2 K for PEG-1000/*N*-EtFOSA/CO_2 systems is shown in Figure S8 in the Supporting Information. Our experiments show that the solubility of PEG-1000 in pure CO_2 in the pressure range of 6–16 MPa is too small to be detected. Therefore, the PEG-1000 can be assumed to be solubilized totally in the reverse micelles. The maximum W_0 value of a PEG-1000/*N*-EtFOSA/CO_2 microemulsion can reach 0.11 at 16.0 MPa and 298.2 K; in this case the weight ratio of the PEG-1000 and the surfactant is equivalent to that of the PEG-400/*N*-EtFOSA/CO_2 microemulsion with a W_0^{corr} value of about 0.28, because the molecular weights of the two PEGs are different. The W_0^{corr} value of the PEG-400/*N*-EtFOSA/CO_2 microemulsion is 0.36 at the same pressure and temperature. Clearly, the PEG with a smaller molecular weight is more readily solubilized in the reverse micelles.

In summary, the PEG domains at the nanometer scale within reverse micelles are formed in CO_2 for the first time. The nanosized PEG domains dispersed in CO_2 has many advantages. First, the size and property of nanosized PEG domains can be tuned by the content of PEG. Second, both PEG and CO_2 are tunable solvents; the properties of PEG can be easily tuned by the molecular weight of PEG. Besides, these two solvents are environmentally benign. All these special features confer the nanosized PEG domains dispersed in CO_2 potential applications in different fields, such as chemical reactions, material synthesis, extraction, and others.

Experimental Section

Materials: The surfactant *N*-EtFOSA (*N*-ethyl perfluorooctylsulfonamide $>95\%$) was purchased from Guangzhou Leelchem Corporation. PEG-400 (A. R. grade) was supplied by Beijing Chemical Reagents Company. PEG-1000 (A. R. grade) was purchased from Sinopharm Chemical Reagent Co., Ltd. Methyl orange (MO) was provided by Beijing Chemical Reagent Company (A. R. grade). CO_2 was supplied by Beijing Analytical Instrument Factory with a purity of $>99.99\%$. $HAuCl_4$ was provided by Shenyang Jinke Reagent Factory, China.

Phase behavior investigation: The apparatus and procedures to determine the phase behaviors of PEG/*N*-EtFOSA/CO_2 systems were similar to those used previously.[29] Very briefly, the apparatus consisted of a high-pressure view cell, the volume of which could be changed in the range of 20–50 mL, a water bath at constant temperature controlled by a YKKY A2 digital temperature controller with the accuracy ± 0.1 K, a high-pressure syringe pump (DB-80), a gas cylinder, a magnetic stirrer, and a pressure gauge that was accurate to ± 0.025 MPa in the pressure range of 0–22 MPa. In

a typical experiment, the desired amounts of PEG and *N*-EtFOSA were loaded into the view cell that was placed in the water bath with constant temperature. After the thermal equilibrium had been reached, the air in the view cell was removed by applying vacuum and CO_2 was charged into the cell under stirring. The minimum pressure at which the mixture became clear (one phase) was defined as the cloud-point pressure. The procedures to determine the solubility of PEG in pure CO_2 was similar. The main difference was that *N*-EtFOSA was not involved.

Small-angle X-ray scattering: The SAXS experiments were carried out at Beamline 4B9A at the Beijing Synchrotron Radiation Facility (BSRF). The wavelength was 1.53 Å, and the distance of sample to detector was 1.68 m. The data were collected using a CCD detector (MAR) with a maximum resolution of 3450×3450 pixels. The detailed description of the apparatus was given elsewhere.[30] It was composed of a stainless-steel body and two diamond windows of 8 mm in diameter and 0.4 mm in thickness. The X-ray path length of the cell was 1.5 mm and the internal volume of the cell was 2.7 mL. In a typical experiment, the suitable amount of *N*-EtFOSA and PEG-400 was added into the high-pressure SAXS cell and air in the cell was removed. Then CO_2 was charged into the cell until the desired pressure was reached. The cell was controlled within ± 0.1 K of the experimental temperature. The pair–distance distribution function $p(r)$ and gyration radius (R_g) were obtained from SAXS data by using an Irena tool suite within the Igor pro application software.[31]

UV/Vis spectra: The apparatus and procedures were similar to those used previously.[32] The apparatus consisted of a gas cylinder, a high-pressure UV sample cell, a high-pressure pump, a pressure gauge, and a temperature controller. The optical path length and the inner volume of the cell were 21 mm and 6.5 mL, respectively. In a typical experiment, the suitable amount of MO/ethanol solution was loaded into the sample cell and the ethanol was removed by blowing nitrogen lightly. The suitable amount of *N*-EtFOSA and PEG was added into the sample cell. Then CO_2 was charged until the desired pressure was reached. The concentration of the probe MO was 4.0×10^{-5} M. The absorbance spectrum was recorded by a TU-1201 Model spectrophotometer (Beijing General Instrument Company).

Au synthesis and characterization: In a typical experiment, surfactant (2.45 g) was added into the high-pressure view cell (49 mL) containing $HAuCl_4$ (0.02 g) and PEG-400 (0.62 g). The high-pressure view cell was placed in a water bath with constant temperature of 298.2 K. Then CO_2 was charged into the cell to the desired pressure (20.20 MPa) under stirring. After reaction for 16 h, CO_2 was released slowly and the products were separated and washed for several times with ethanol. The morphologies of the products were characterized by TEM (JEOL JEM-2010). XRD analysis was performed on an X-ray diffractometer (Model D/MAX2500, Rigaka) with Cu Ka radiation at a scanning rate of $2° \text{min}^{-1}$. Au nanoparticles were dispersed with ethanol and were detected by a TU-1201 Model spectrophotometer (Beijing General Instrument Company).

Received: August 2, 2012
Published online: October 26, 2012

Keywords: carbon dioxide · gold · micelles · supercritical fluids · surfactants

[1] M. Youssef, R. J. M. Pellenq, B. Yildiz, *J. Am. Chem. Soc.* **2011**, *133*, 2499.

[2] a) B. Baruah, J. M. Roden, M. Sedgwick, N. M. Correa, D. C. Crans, N. E. Levinger, *J. Am. Chem. Soc.* **2006**, *128*, 12758; b) N. E. Levinger, L. C. Rubenstrunk, B. Baruah, D. C. Crans, *J. Am. Chem. Soc.* **2011**, *133*, 7205.

[3] a) S. R. K. Minkler, B. H. Lipshutz, N. Krause, *Angew. Chem.* **2011**, *123*, 7966; *Angew. Chem. Int. Ed.* **2011**, *50*, 7820; b) L. C. Lee, Y. Zhao, *Org. Lett.* **2012**, *14*, 784.

[4] a) J. Jang, J. Bae, *Angew. Chem.* **2004**, *116*, 3891; *Angew. Chem. Int. Ed.* **2004**, *43*, 3803; b) E. M. Lambert, C. Viravaidya, M. Li, S. Mann, *Angew. Chem.* **2010**, *122*, 4194; *Angew. Chem. Int. Ed.* **2010**, *49*, 4100; c) W. Kwon, S.-W. Rhee, *Chem. Commun.* **2012**, *48*, 5256.

[5] a) A. I. Cooper, J. D. Londono, G. Wignall, J. B. McClain, E. T. Samulski, J. S. Lin, A. Dobrynin, M. Rubinstein, A. L. C. Burke, J. M. J. Frechet, J. M. DeSimone, *Nature* **1997**, *389*, 368; b) J. A. Gomez del Rio, D. G. Hayes, *Biotechnol. Prog.* **2011**, *27*, 1091.

[6] P. S. W. Yeung, P. H. Axelsen, *J. Am. Chem. Soc.* **2012**, *134*, 6061.

[7] a) H. X. Gao, J. C. Li, B. X. Han, W. N. Chen, J. L. Zhang, R. Zhang, D. D. Yan, *Phys. Chem. Chem. Phys.* **2004**, *6*, 2914; b) J. Eastoe, S. Gold, S. E. Rogers, A. Paul, T. Welton, R. K. Heenan, I. Grillo, *J. Am. Chem. Soc.* **2005**, *127*, 7302; c) J. H. Liu, S. Q. Cheng, J. L. Zhang, X. Y. Feng, X. G. Fu, B. X. Han, *Angew. Chem.* **2007**, *119*, 3377; *Angew. Chem. Int. Ed.* **2007**, *46*, 3313; d) S. Q. Cheng, J. L. Zhang, Z. F. Zhang, B. X. Han, *Chem. Commun.* **2007**, 2497; e) A. Chandran, K. Prakash, S. Senapati, *J. Am. Chem. Soc.* **2010**, *132*, 12511; f) D. D. Ferreyra, N. M. Correa, J. J. Silber, R. D. Falcone, *Phys. Chem. Chem. Phys.* **2012**, *14*, 3460.

[8] P. Setua, R. Pramanik, S. Sarkar, C. Ghatak, V. G. Rao, N. Sarkar, S. K. Das, *J. Mol. Liq.* **2011**, *162*, 33.

[9] F. Gayet, C. El Kalamouni, P. Lavedan, J. D. Marty, A. Brulet, N. Lauth-de Viguerie, *Langmuir* **2009**, *25*, 9741.

[10] a) A. Zaki, N. Dave, J. Liu, *J. Am. Chem. Soc.* **2012**, *134*, 35; b) B. Obermeier, F. Wurm, C. Mangold, H. Frey, *Angew. Chem.* **2011**, *123*, 8136; *Angew. Chem. Int. Ed.* **2011**, *50*, 7988.

[11] a) X. F. Yang, J. X. Fu, C. J. Jin, J. A. Chen, C. L. Liang, M. M. Wu, W. Z. Zhou, *J. Am. Chem. Soc.* **2010**, *132*, 14279; b) X. M. Qian, X. Zhou, S. M. Nie, *J. Am. Chem. Soc.* **2008**, *130*, 14934.

[12] D. J. Heldebrant, P. G. Jessop, *J. Am. Chem. Soc.* **2003**, *125*, 5600.

[13] a) A. Méndez, L. E. Moron, L. Ortiz-Frade, Y. Meas, R. Ortega-Borges, G. Trejo, *J. Electrochem. Soc.* **2011**, *158*, F45; b) Y. Kato, T. Ishihara, H. Ikuta, Y. Uchimoto, M. Wakihara, *Angew. Chem.* **2004**, *116*, 2000; *Angew. Chem. Int. Ed.* **2004**, *43*, 1966.

[14] K. Knop, R. Hoogenboom, D. Fischer, U. S. Schubert, *Angew. Chem.* **2010**, *122*, 6430; *Angew. Chem. Int. Ed.* **2010**, *49*, 6288.

[15] a) C. A. Eckert, B. L. Knutson, P. G. Debenedetti, *Nature* **1996**, *383*, 313; b) E. J. Beckman, *Science* **1996**, *271*, 613; c) G. B. Jacobson, C. T. Lee, K. P. Johnston, W. Tumas, *J. Am. Chem. Soc.* **1999**, *121*, 11902; d) A. I. Cooper, *Adv. Mater.* **2003**, *15*, 1049; e) B. Tan, J. Y. Lee, A. I. Cooper, *Macromolecules* **2006**, *39*, 7471; f) P. G. Jessop, B. Subramaniam, *Chem. Rev.* **2007**, *107*, 2666; g) Q. L. Chen, E. J. Beckman, *Green Chem.* **2008**, *10*, 934; h) J. W. Ford, M. E. Janakat, J. Lu, C. L. Liotta, C. A. Eckert, *J. Org. Chem.* **2008**, *73*, 3364; i) C. A. Kelly, A. Naylor, L. Illum, K. M. Shakesheff, S. M. Howdle, *Adv. Funct. Mater.* **2012**, *22*, 1684.

[16] a) D. Gourgouillon, M. N. da Ponte, *Phys. Chem. Chem. Phys.* **1999**, *1*, 5369; b) J. A. Lopes, D. Gourgouillon, P. J. Pereira, A. M. Ramos, M. N. da Ponte, *J. Supercrit. Fluids* **2000**, *16*, 261; c) M. Daneshvar, S. Kim, E. Cular, *J. Phys. Chem.* **1990**, *94*, 2124.

[17] a) A. Dupont, J. Eastoe, L. Martin, *Langmuir* **2004**, *20*, 9960; b) J. Y. Park, J. S. Lim, Y. W. Lee, K. P. Yoo, *Fluid Phase Equilib.* **2006**, *240*, 101.

[18] a) J. L. Zhang, B. X. Han, J. C. Liu, X. G. Zhang, G. Y. Yang, J. He, Z. M. Liu, T. Jiang, J. Wang, B. Z. Dong, *J. Chem. Phys.* **2003**, *118*, 3329; b) Y. J. Zhao, J. L. Zhang, Q. Wang, W. Li, J. S. Li, B. X. Han, Z. H. Wu, K. H. Zhang, Z. H. Li, *Langmuir* **2010**, *26*, 4581.

[19] a) K. Debbabi, F. Guittard, J. Eastoe, S. Rogers, S. Geribaldi, *Langmuir* **2009**, *25*, 8919; b) M. Hirai, R. Kawai-Hirai, S. Yabuki, T. Takizawa, T. Hirai, K. Kobayashi, Y. Amemiya, M. Oya, *J. Phys. Chem.* **1995**, *99*, 6652; c) M. Hirai, R. Kawai-Hirai, M. Sanada, H. Iwase, S. Mitsuya, *J. Phys. Chem. B* **1999**, *103*, 9658;

d) X. G. Zhang, Y. J. Chen, J. X. Liu, C. Z. Zhao, H. J. Zhang, *J. Phys. Chem. B* **2012**, *116*, 3723.
[20] a) J. Brunner-Popela, R. Mittelbach, R. Strey, K. V. Schubert, E. W. Kaler, O. Glatter, *J. Chem. Phys.* **1999**, *110*, 10623; b) L. K. Shrestha, O. Glatter, K. Aramaki, *J. Phys. Chem. B* **2009**, *113*, 6290; c) L. K. Shrestha, R. G. Shrestha, D. Varade, K. Aramaki, *Langmuir* **2009**, *25*, 4435.
[21] a) R. G. Zielinski, S. R. Kline, E. W. Kaler, N. Rosov, *Langmuir* **1997**, *13*, 3934; b) J. Eastoe, B. M. H. Cazelles, *Langmuir* **1997**, *13*, 6980.
[22] M. J. Clarke, K. L. Harrison, K. P. Johnston, S. M. Howdle, *J. Am. Chem. Soc.* **1997**, *119*, 6399.
[23] a) O. Aschenbrenner, P. Styring, *Energy Environ. Sci.* **2010**, *3*, 1106; b) J. Li, Y. M. Ye, L. F. Chen, Z. W. Qi, *J. Chem. Eng. Data* **2012**, *57*, 610; c) T. Guadagno, S. G. Kazarian, *J. Phys. Chem. B* **2004**, *108*, 13995; d) I. Pasquali, J.-M. Andanson, S. G. Kazarian, R. Bettini, *J. Supercrit. Fluids* **2008**, *45*, 384.
[24] K. P. Johnston, K. L. Harrison, M. J. Clarke, S. M. Howdle, M. P. Heitz, F. V. Bright, C. Carlier, T. W. Randolph, *Science* **1996**, *271*, 624.
[25] a) H. Y. Liang, W. Z. Wang, Y. Z. Huang, S. P. Zhang, H. Wei, H. X. Xu, *J. Phys. Chem. C* **2010**, *114*, 7427; b) Y. Hatakeyama, T. Morita, S. Takahashi, K. Onishi, K. Nishikawa, *J. Phys. Chem. C* **2011**, *115*, 3279.
[26] a) T. Shimizu, T. Teranishi, S. Hasegawa, M. Miyake, *J. Phys. Chem. B* **2003**, *107*, 2719; b) K. Y. Lee, J. Hwang, Y. W. Lee, J. Kim, S. W. Han, *J. Colloid Interface Sci.* **2007**, *316*, 476.
[27] a) J. L. Zhang, Y. J. Zhao, J. S. Li, G. Y. Yang, B. X. Han, Z. H. Wu, Z. H. Li, *Soft Matter* **2010**, *6*, 6200; b) J. He, M. T. Perez, P. Zhang, Y. J. Liu, T. Babu, J. L. Gong, Z. H. Nie, *J. Am. Chem. Soc.* **2012**, *134*, 3639.
[28] a) E. Weidner, V. Wiesmet, Z. Knez, M. Skerget, *J. Supercrit. Fluids* **1997**, *10*, 139; b) J. Y. Hao, M. J. Whitaker, G. Serhatkulu, K. M. Shakesheff, S. M. Howdle, *J. Mater. Chem.* **2005**, *15*, 1148; c) I. Pasquali, L. Comi, F. Pucciarelli, R. Bettini, *Int. J. Pharm.* **2008**, *356*, 76.
[29] B. Wang, J. He, D. H. Sun, R. Zhang, B. X. Han, *Fluid Phase Equilib.* **2006**, *239*, 63.
[30] J. L. Zhang, B. X. Han, Y. J. Zhao, W. Li, Y. Liu, *Phys. Chem. Chem. Phys.* **2011**, *13*, 6065.
[31] a) Y. J. Zhao, J. L. Zhang, B. X. Han, S. Q. Hu, W. Li, *Green Chem.* **2010**, *12*, 452; b) J. S. Li, J. L. Zhang, B. X. Han, L. Peng, G. Y. Yang, *Chem. Commun.* **2012**, *48*, 10562.
[32] J. L. Zhang, B. X. Han, Y. J. Zhao, J. S. Li, G. Y. Yang, *Chem. Eur. J.* **2011**, *17*, 4266.

